at energies corresponding to the same momentum transfer. The change of that requirement in more complete theories may lead to better agreement in the Chew-Low extrapolation. An alternative way of improving the calculation might be the replacement of the term $\sigma(E, \theta)$ in Eq. (1) by the off-energy-shell scattering cross section. A series of measurements carried out at other angles where the various effects have different separations would throw light on the questions about interference, while a series carried out at a fixed set of angles at different energies both below and above the present one would be of interest, since the change of incident energy is probably the best way of moving the scattering process to different depths off the energy shell. Sets of such experiments, besides their value for the appraisal of the approximate treatment, would be helpful for a comparison with exact solutions of the proton-induced deuteron breakup developed along the lines of the recent works of Schulman[23] and of Noble.[24]

CONCLUSIONS

(1) The fact that the QFS process is strongly related to the energy of the spectator particle has been demonstrated.

(2) The shape of the measured spectra are satisfactorily fitted by the spectator model.

(3) The noncoplanar experiment demonstrates that the quasifree process tends to be coplanar except for the broadening allowed by the target internal wave function.

(4) Within the frame of the SIA approach, it has not been possible to explain the absolute cross sections. A Chew-Low extrapolation attempt is partially successful in relating the observed cross sections to the free scattering cross sections, but also indicates that other effects enter.

(5) The results should be compared with further calculations including interference and FSI terms. This will necessitate an examination of various degrees of approximation, including the Born approximation.

(6) The dependence of the cross section on off-energy-shell effects should be examined. Although there is no direct evidence that these are important, they remain an important unknown factor.

ACKNOWLEDGMENTS

It is our pleasure to express our gratitude to Dr. J. M. Cameron for help in the calculations, Dr. R. E. Warner for helpful discussion, T. Woods for participating in the measurements, and to the staff of the UCLA cyclotron for its operation of the machine.

[23] L. Schulman, Phys. Rev. **156**, 1129 (1967).
[24] J. V. Noble, Phys. Rev. **161**, 945 (1967).

PHYSICAL REVIEW VOLUME 188, NUMBER 4 20 DECEMBER 1969

^{14}N-^{14}N and ^{14}N-^{16}O Elastic Scattering*

L. A. JACOBSON†
University of Wisconsin, Madison, Wisconsin 53706

(Received 5 August 1969)

We report differential cross sections at 40–50 angles (35°–110° c.m.) for ^{14}N-^{14}N and ^{14}N-^{16}O elastic scattering. The c.m. energies vary in steps of 200 keV from 5 MeV to ~18 MeV. For ^{14}N-^{14}N, some additional data extend to ~20 MeV. Only at the lower energies does either the optical model or a modified diffraction model satisfactorily describe the data. At the higher energies, weak but broad peaks appear in the excitation curves. Evidence concerning finer structure is inconclusive.

INTRODUCTION

RECENTLY, we have made extensive measurements on ^{14}N-^{14}N and ^{14}N-^{16}O elastic scattering and have employed both a modified Blair model[1] and an optical model to describe the data. Subsequent to our analysis, other models have been proposed to describe heavy-ion elastic scattering.[2–4]

The only other data on ^{14}N-^{14}N scattering are those of Reynolds and Zucker,[5] who measured the differential

* Work supported in part by the U. S. Atomic Energy Commission.
† Present address: Schlumberger, 5000 Gulf Freeway, Houston, Tex.
[1] J. S. Blair, Phys. Rev. **95**, 1218 (1954).
[2] W. Scheid, R. Ligensa, and W. Greiner, Phys. Rev. Letters **21**, 1497 (1968).
[3] K. A. Brueckner, J. R. Buchler, and M. M. Kelly, Phys. Rev. **173**, 944 (1968).
[4] R. J. Munn, B. Block, and F. B. Malik, Phys. Rev. Letters **21**, 159 (1968); L. Rickersten, B. Block, J. W. Clark, and F. B. Malik, *ibid.* **22**, 951 (1969).
[5] H. L. Reynolds and A. Zucker, Phys. Rev. **102**, 1398 (1956).

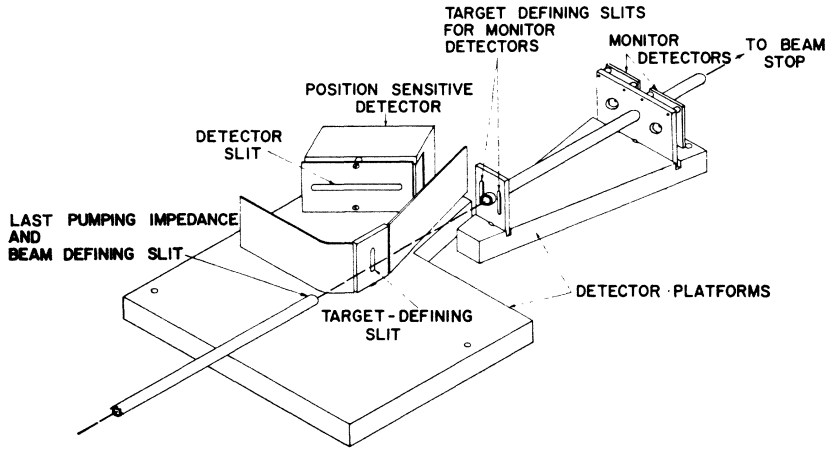

FIG. 1. Schematic view of the interior of the gas-scattering chamber, showing slit and detector arrangements.

cross section for elastic scattering at four energies, two above the Coulomb barrier and two below. They applied the Blair model to only their highest-energy data (at 10.85 MeV)[6] and found a radius parameter r_0 of 1.66 fm. Subsequently, Porter[7] analyzed the same data employing an optical model with a Wood-Saxon complex well. Parameter sets corresponding to real well depths of 20 and 40 MeV gave equally good descriptions of the data.

Heavy-ion elastic scattering has been studied for other projectiles and targets.[8] Of particular interest are the results on ^{12}C-^{12}C, ^{12}C-^{16}O, and ^{16}O-^{16}O scattering.[9,10] Above the Coulomb barrier, the ^{12}C-^{12}C scattering revealed sizable fluctuations in the cross sections of several hundred keV width. The ^{12}C-^{16}O scattering revealed some structure above 13 MeV, and the ^{16}O-^{16}O scattering at energies above 17 MeV revealed broad, evenly spaced peaks with peak-to-valley ratios of 10:1, and considerable fine structure.

An optical-model analysis[10] of the high-energy ^{16}O-^{16}O scattering data reproduced the general trend of the peaks by using a shallow potential (~17 MeV), but could not produce the large peak-to-valley ratio observed. A potential with both a repulsive real core at short range and an absorbing core[4] will generate the large peak-to-valley ratio observed. Since the ^{12}C-^{12}C scattering and ^{16}O-^{16}O scattering appear to be somewhat different, while the ^{12}C-^{16}O scattering tends to exhibit features of both, we chose to investigate more carefully ^{14}N-^{14}N scattering and also to look at ^{14}N-^{16}O scattering.

EXPERIMENTAL APPARATUS AND DATA REDUCTION

Ammonia gas in a direct-extraction duoplasmatron ion source produced an intense NH_2^- beam,[11] of which an EN tandem accelerator would accept about 1 μA. The emerging high-energy nitrogen beam ($N^{+3,4,5,6}$) yielded

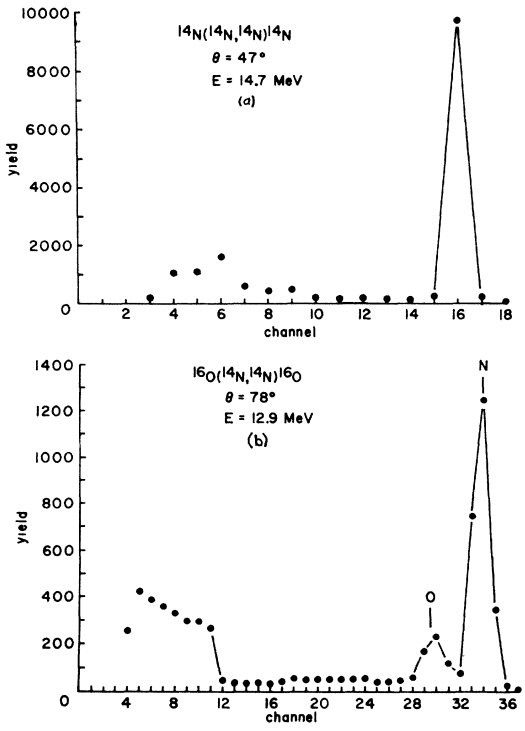

FIG. 2. Typical pulse-height spectra for (a) ^{14}N-^{14}N and (b) ^{14}N-^{16}O scattering. The high yield immediately above the low-energy cutoff (channels 3–9 and 4–11) comes from partially stopped light ions. The energy calibration is ~1.4 MeV/channel for the ^{14}N-^{14}N data and ~0.4 MeV/channel for the ^{14}N-^{16}O data.

[6] Throughout this paper, all cross sections, angles, and energies are measured in the c.m. system unless otherwise noted. In the case of nonidentical particles, the measurements refer to the scattered projectile.

[7] C. E. Porter, Phys. Rev. **112**, 1722 (1958).

[8] For an extensive list of references to heavy-ion work prior to 1965, see K. R. Greider, Ann. Rev. Nucl. Sci **15**, 291 (1965). For more recent work, see A. Gobbi, U. Matter, J. L. Perrenoud, and P. Marmier, Nucl. Phys. **A112**, 537 (1968).

[9] D. A. Bromley, J. A. Kuehner, and E. Almqvist, Phys. Rev. **123**, 878 (1961).

[10] R. H. Seimssen, J. V. Maher, A. Weidinger, and D. A. Bromley, Phys. Rev. Letters **19**, 369 (1967).

[11] L. A. Jacobson, Ph.D. dissertation, 1969 (unpublished), available through University Microfilms, Ann Arbor, Mich.

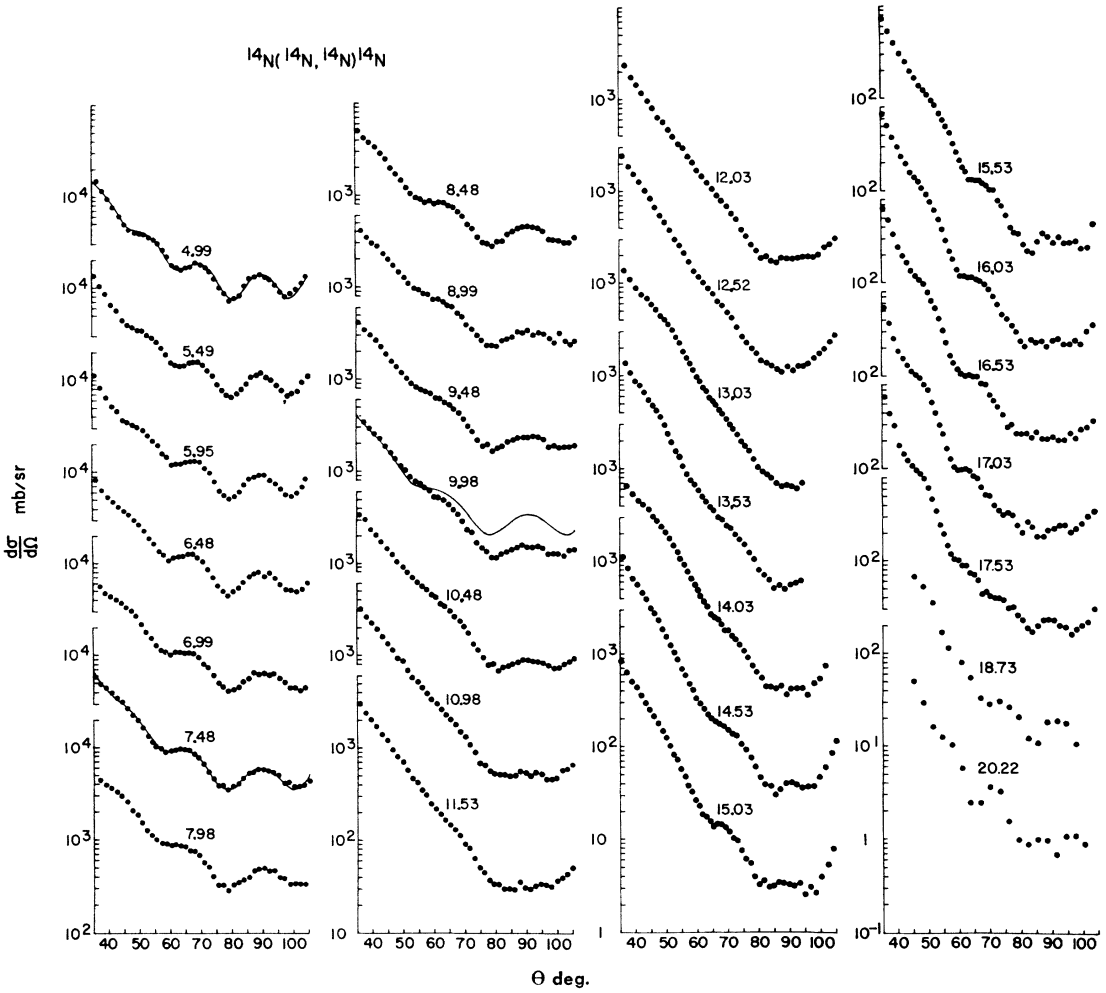

FIG. 3. Samples of the ^{14}N–^{14}N differential cross sections. (Intermediate data in 100-keV steps are available.) Each curve (labeled by c.m. energy) is displaced from the one below it by a factor of 10. The dot size represents approximately $\frac{1}{2}$ the angular resolution of the detection system and a magnitude uncertainty of ±5%. For the smallest cross sections of a few mb/sr, the data uncertainty is about twice the dot size. The solid lines at 4.99, 7.48, and 9.98 MeV are the Coulomb (Mott) scattering prediction. All quantities refer to c.m. system.

0.3-μA to 10-nA flux through a differentially pumped gas-scattering chamber.[11,12]

A position-sensitive detector[13] (PSD), set to span a c.m. angular range of approximately 35°–110°, detected the scattered particles (see Fig. 1).

A pair of diffused junction silicon detectors located at ±5° (lab) monitors the product of the beam flux and the gas density.

The energy and position-related signals from the PSD after conversion to digital form, enter an on-line computer (Honeywell DDP-124). The computer removes the energy dependence of the position-related signal (equal to xE, where x is the linear position), produces a two-parameter yield array of energy versus position, and stores the array on magnetic tape for subsequent analysis. The array for the ^{14}N-^{14}N scattering had 32 channels along the energy axis (except for some very low-energy runs where only 16 channels were used). For the ^{14}N-^{16}O scattering the energy axis had 64 channels. The position axis had 64 channels for all work except the five angular distributions of ^{14}N-^{14}N scattering at 18.25, 18.75, 19.25, 19.75, and 20.25 MeV, where 32 channels were used. Figures 2(a) and 2(b) show typical energy pulse-height spectra for ^{14}N-^{14}N and ^{14}N-^{16}O scattering at selected position channels (shown converted to angle).

For data reduction a semiautomatic computer code sums the elastic ^{14}N events, makes an appropriate background subtraction, corrects for nonlinearity effects in the position detector, and outputs an angular dis-

[12] P. Tollefsrud, Ph.D. dissertation, 1969 (unpublished), available through University Microfilms, Ann Arbor, Mich.

[13] Nuclear Triode, Nuclear Diodes Inc., Prairie View, Ill., Model NTC-450-120.

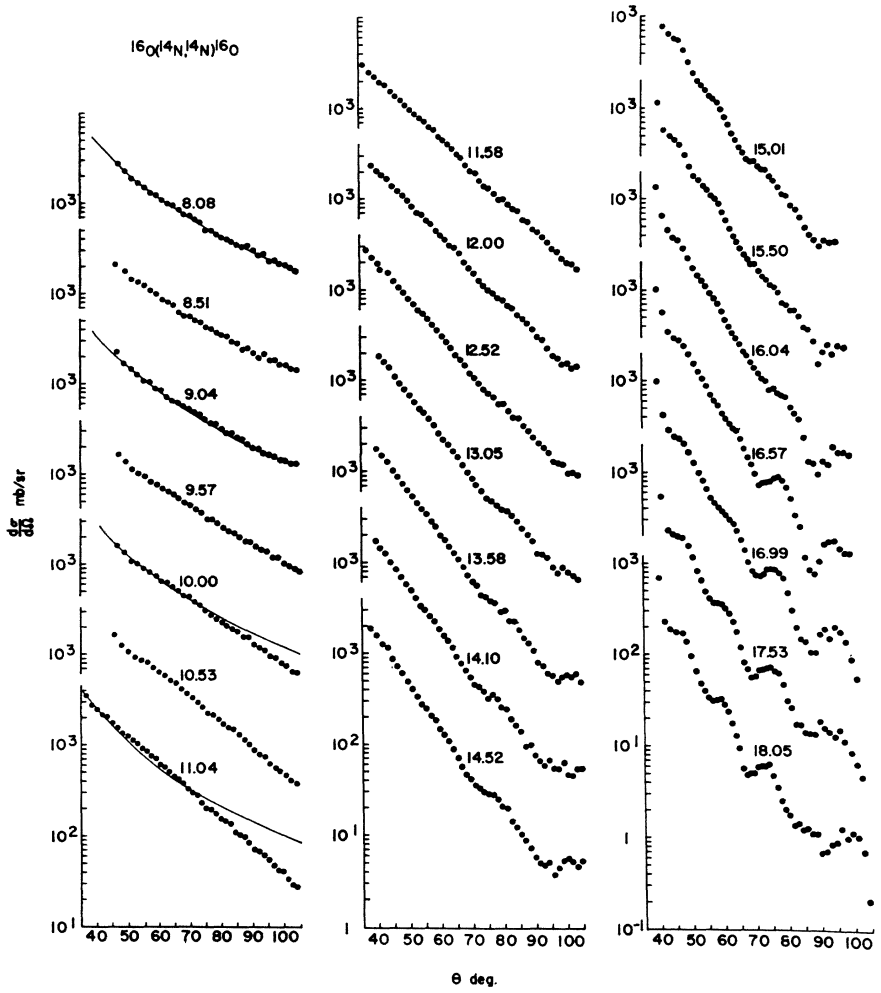

FIG. 4. Samples of the ^{14}N-^{16}O differential cross sections (intermediate data in 100-keV steps are available). Each curve (labeled by its c.m. energy) is displaced from the one below it by a factor of 10. The dot size represents approximately $\frac{1}{2}$ the angular resolution of the detection system and a magnitude uncertainty of $\pm 5\%$. For the smallest cross sections of $\sim$1 mb/sr, uncertainties are 2–3 times the dot size. The solid lines at 8.08, 9.04, 10.00 and 11.04 MeV are the Coulomb scattering prediction. All quantities refer to c. m. system.

tribution. We measured the linearity of the position detection by taking data with 20 evenly spaced slots in front of the detector and then noting the channel location of the centers of the groups which arise from the 20 slots.

By varying the depletion depth of the PSD (45–100 μ), we could optimize the heavy-ion elastic peak with respect to the background as a function of energy and angle. The ^{14}N-^{14}N data were free of resolution problems except for possible low Q-value neutron and proton transfer reactions, $^{14}N(^{14}N, ^{13}N)^{15}N$ and $^{14}(^{14}N, ^{13}C)^{15}O$. However, these two reactions have been extensively studied at energies <10 MeV, and less so at higher energies.[14–17] Since the total cross section for both of these is less than 6 mb at high energy and the angular distributions are strongly forward peaked, we conclude that no significant contribution to the elastic events would arise from these processes.

Thus, summing over the ^{14}N elastic group for the ^{14}N-^{14}N scattering and making a suitable background subtraction are straightforward.

For ^{14}N-^{16}O scattering, the ^{16}O elastic recoil peak falls just below the elastic ^{14}N peak [see Fig. 2(b)]. The separation between the two is maximum at backward angles, and becomes small at forward angles. Forward of 60°, we could never clearly separate the two elastic peaks; the recoil ^{16}O peak appears as a small shoulder on the low-energy side of the scattered ^{14}N peak. Fortunately, the recoil ^{16}O yield (relative to the ^{14}N yield) decreases rapidly as the angle decreases. This behavior results from the fact that forward-recoiling ^{16}O corresponds to back-scattered ^{14}N. Where Coulomb scattering dominates, the back scattered ^{14}N decreases as $\sin^4\frac{1}{2}\theta$. For such a case, we expect the ratio of the ^{16}O yield to ^{14}N yield would be about 0.1 at 60° (taking into account the c.m. to laboratory conversion) and decreasing to less than 0.01 at 35°. At higher energies, where nuclear effects are expected to dominate, our results (Figs. 5 and 6) indicate that the ^{14}N cross sections at intermediate angles (60°–110°, where separation is adequate) are always much less than

[14] J. C. Heibert, J. A. McIntyre, and J. G. Couch, Phys. Rev. **138**, B346 (1965).
[15] R. M. Gaedke, K. S. Toth, and I. R. Williams, Phys. Rev. **141**, 996 (1966).
[16] F. C. Jobes and J. A. McIntyre, Phys. Rev. **133**, B893 (1964).
[17] H. L. Reynolds and A. Zucker, Phys. Rev. **101**, 166 (1956).

Rutherford, so the resultant ^{16}O contaminant of the corresponding angle ^{14}N peak should be even less important.

Thus, while we have not measured the ^{14}N scattering cross section from 120° to 145° (which gives the ^{16}O recoils 60°–35°) the ^{14}N yield at somewhat smaller angles gives us confidence that the Coulomb scattering assumption would be an upper limit for the ^{16}O contaminant to the forward-angle ^{14}N peaks. No more than 10% error would be introduced at 60° by inclusion of the ^{16}O recoils; furthermore, this limit decreases to 1% at 35°. For our ^{14}N yield, we exclude the shoulder caused by the ^{16}O recoils; thus, we expect that the error introduced by the ^{16}O recoil events is small.

The angular range of the detector is calibrated by aligning the interference pattern in the ^{14}N-^{14}N yield-versus-channel array with the theoretical interference pattern for scattering of identical particles at an energy below the Coulomb barrier. The cross section at all other energies is related to the cross section at the calibration energy (7.48 MeV for the ^{14}N-^{14}N data and 7.96 MeV for the ^{14}N-^{16}O data) by the expression

$$\sigma(E,\theta)=\sigma(E_0,\theta)\times\frac{Y(E,\theta)}{Y(E_0\theta)}\times\frac{Y_m(E_0)}{Y_m(E)}\times\left(\frac{E_0}{E}\right)^2,$$

where $\sigma(E_0,\theta)$ is the Coulomb differential cross section at calibration energy E_0 and angle θ and $Y(E,\theta)$ is the elastic yield at E for $Y_m(E)$ counts in the monitor counters at 5° (lab). For Coulomb scattering at $\theta=$ 5° (lab), the quantity Y_mE^2 measures the product of the number of incident particles and the average target density.

The target-defining slit width, the distance from the target-defining slit to the detector, and the detectors' intrinsic position resolution [measured for 15-MeV (lab) ^{14}N ions to be 0.5 mm full width at half-maximum (FWHM)] result in an angular resolution of ±2.2° typically. The angular uncertainty that arises in our data-reduction procedure is ±1.8° and is systematic within any single angular distribution. The total uncertainty of the differential cross section is small at small angles (usually less than 1.5%), but because of the small cross section at large angles and high energy, the statistical errors rise to ~10% for the high-energy backward-angle data. The energy uncertainty is ±0.5%. See Ref. 11 for more detail on the sources of error.

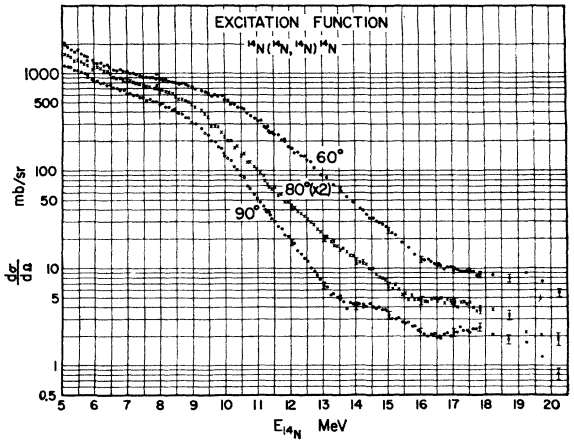

FIG. 5. ^{14}N–^{14}N excitation function at 3 angles. The 80° curve is displaced upward by a factor of 2. The data were obtained from the angular distributions by interpolation between data points straddling the desired angle. Where the uncertainties exceed the symbol size, error bars are indicated every MeV. All quantities refer to c.m. system.

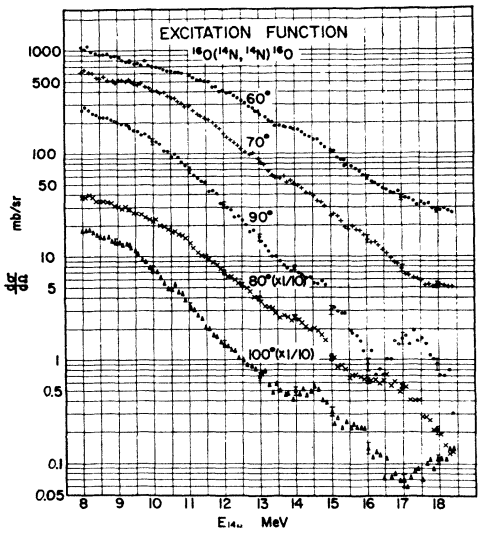

FIG. 6. ^{14}N–^{16}O excitation function for 5 angles. The 80° and 100° data are displaced downward by one decade. The values plotted were obtained in the same manner as the ^{14}N–^{14}N excitation curves, except in the energy range 13.5–15.0 MeV at 100°, where the values involve extrapolation from the 97° data. Where the data uncertainty exceeds the symbol size, error bars are indicated every MeV. All quantities refer to c.m. system.

RESULTS

For the ^{14}N-^{14}N scattering process, we recorded simultaneously the differential cross sections for 40–50 angles. We varied the incident energy in 100-keV steps 5–17.7 MeV, and in 500-keV steps 18.25–20.25 MeV. We recorded similar data in 100-keV steps 8–18.3 MeV for ^{14}N-^{16}O scattering. The target thickness varied from 4 keV at low energies to 36 keV at the high energies. Since the cross sections changed only slowly with energy, we display only the data taken at every half MeV in Figs. 3 and 4. Figures 5 and 6 show excitation functions obtained from the angular distribution data.

Several features are noteworthy: The 90° excitation for ^{14}N-^{14}N indicates two broad but highly attenuated peaks between 13 and 20 MeV. The 90° excitation function of the ^{14}N-^{16}O data shows at least one broad peak between 16 and 18 MeV, and perhaps a less-pronounced peak between 13.5 and 15.5 MeV. There may be some finer structure of 100–200 keV width present in the ^{14}N-^{16}O data, but the statistics are such that the evidence is not conclusive. For both scattering

TABLE I. ^{14}N-^{14}N data.

Optical-model parameters $r_0=1.5$ fm, $a_0=0.5$ fm			
E (MeV)	U (MeV)	W (MeV)	χ^2
14.6	15.0	6.2	5.0
14.6	24.0	10.0	7.6
16.2	26.1	10.5	15.0
17.7	29.4	11.8	21.0

Diffraction-model parameters				
E (MeV)	r_0 (fm)	a	Δ	χ^2
9.6	1.7	0.07	...	6.4
11.1	1.72	0.09	...	4.9
12.5	1.72	0.11	...	4.3
14.6	1.70	0.07	0.6	7.8
15.2	1.70	0.07	0.5	7.5
16.2	1.70	0.07	0.6	24.1
17.4	1.68	0.06	0.6	22.7
17.7	1.65	0.07	0.6	25.9

processes the measured cross section falls far below the Coulomb scattering prediction as we go to higher energies.

Siemssen *et al.*[10] observed very striking broad structure in the ^{16}O-^{16}O scattering above 15 MeV, which had a peak-to-valley ratio of 10:1. We have observed a peak-to-valley ratio of 3:1 for the ^{14}N-^{16}O scattering but only a very small 5:4 ratio for the ^{14}N-^{14}N scattering. This small ratio may simply reflect the large number of channels open in the ^{14}N-^{14}N interaction.

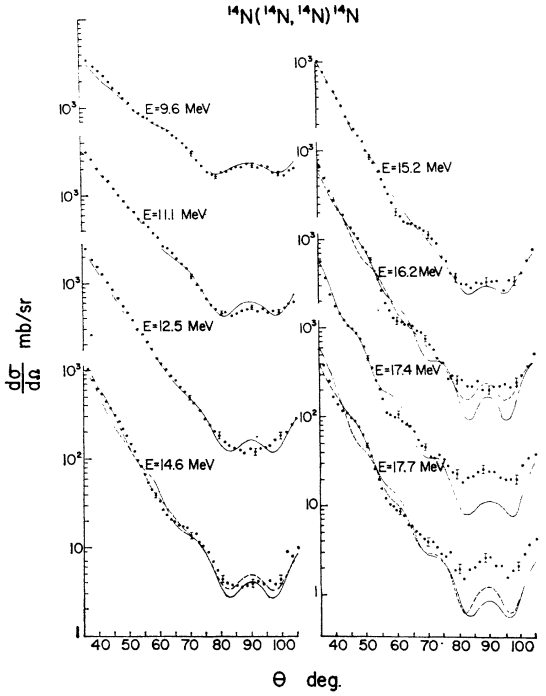

FIG. 7. Diffraction-model curves (solid lines) and optical-model curves (dashed lines) for the parameters shown in Table I. The optical-model fit at 14.6 MeV is for the second parameter set shown in Table I.

ANALYSIS—OPTICAL MODEL

The ^{14}N-^{14}N and ^{14}N-^{16}O data were analyzed using an optical-model code[18] employing a standard Wood-Saxon potential with the four parameters U, W, r_0, and a.

For input parameters we usually started with those of older ^{14}N-^{14}N studies[7,19] or other heavy-ion data,[10] though we experimented some with other quite arbitrary starting values.

Table I shows the parameters which produced the best fits for the higher-energy data, and Fig. 7 shows the fits (dashed lines). An average χ^2 per point of 1 is a fit to within the errors of the data. As can be seen, at no energy did we find really satisfactory fits, with the exception perhaps of 14.6 MeV. The addition of other parameters such as a separate radius and diffuseness for the imaginary potential did not result in significantly improved fits. No spin-orbit interaction was assumed.

TABLE II. ^{14}N-^{16}O data.

Optical-model parameters $a_0=0.5$ fm				
E (MeV)	U (MeV)	W (MeV)	r_0 (fm)	χ^2
14.0	10.1	3.0	1.4	12.
17.0	14.1	4.0	1.35	4.8
18.3	10.6	3.3	1.4	15.

Diffraction-model parameters $r_0=1.65$ fm, $a=0.05$, $\Delta=0.9$					
E (MeV)	χ^2	E (MeV)	χ^2	E (MeV)	χ^2
12.0	6.3	15.0	4.3	18.0	8.0
13.0	4.7	16.0	14.5	18.3	15.4
14.0	8.9	17.0	8.8		

We performed an extensive parameter search only for the 18.3-MeV ^{14}N-^{16}O data. Besides the parameters found from the ^{14}N-^{14}N analysis, potentials in the range $U=10$–100 MeV and $W=3$–30 MeV were investigated. Table II and Fig. 8 display results of the parameter search. The optical-model searches at 17.0 and 14.0 MeV started with the 18.3-MeV parameters.

Since it is questionable whether an optical model is a relevant description of the colliding system, we have not tried to refine further the calculations.

[18] The code OPTIX was originally written by Thompson and Gille of Florida State University, modified and improved by P. Schwandt of the University of Wisconsin, and adapted to identical-particle scattering by the author.

[19] G. Breit, J. A. Polak, and D. A. Torchia, Phys. Rev. **161**, 993 (1967).

ANALYSIS—DIFFRACTION MODEL

Blair's original sharp-cutoff model,[1] which was first applied to heavy-ion scattering by Reynolds and Zucker,[5] has since been modified in several ways.[9,20,21] We have used two modifications, a rounded cutoff in the absorption and a real nuclear phase shift for L waves corresponding to surface interactions. If we neglect spin effects and expand the nuclear scattering amplitude $f_n(\theta)$ in partial waves, we have

$$f_n(\theta)=k^{-1}\sum_{L=0}^{L\max}(2L+1)\alpha_L P_L(\cos\theta)e^{2i\omega_L},$$

where

$\omega_L=\sigma_L-\sigma_0$, σ_L is the Coulomb phase,

$\alpha_L=(1/2i)(e^{2i\delta_L}-1)$, and δ_L is the nuclear phase.

We parametrized α_L as

$$\mathrm{Re}\alpha_L=0.5(1-A_L)\sin 2\delta_L{}^R,$$

$$\mathrm{Im}\alpha_L=0.5[1-(1-A_L)\cos 2\delta_L{}^R],$$

where

$$A_L=\{1+\exp[(L-L_{\mathrm{cut}})/aL_{\mathrm{cut}}]\}^{-1},$$

$$\delta_L{}^R=(\Delta/2)\exp[(L-L_{\mathrm{cut}})/aL_{\mathrm{cut}}]A_L{}^2,$$

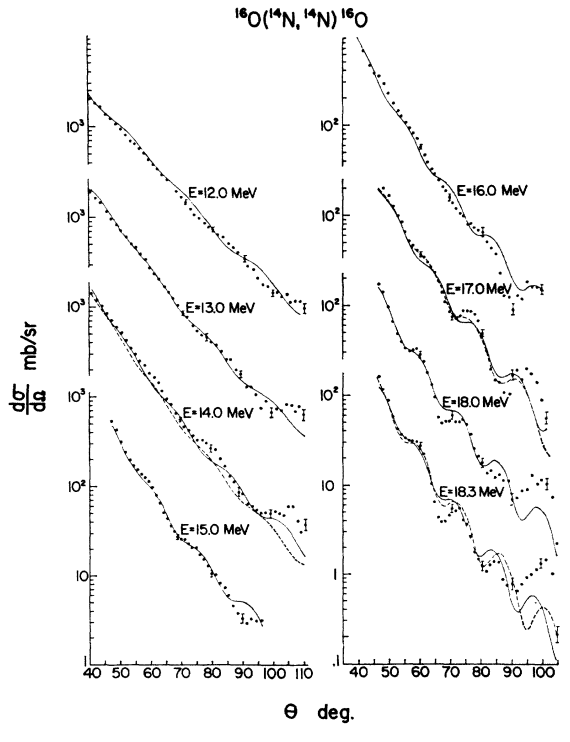

FIG. 8. Diffraction-model curves (solid line) and optical-model curves (dashed line) for the parameters shown in Table II.

[20] J. A. McIntyre, K. H. Wang, and L. C. Beckner, Phys. Rev. 117, 1337 (1960).
[21] J. S. McIntosh, S. C. Park, and J. E. Turner, Phys. Rev. 117, 1284 (1960).

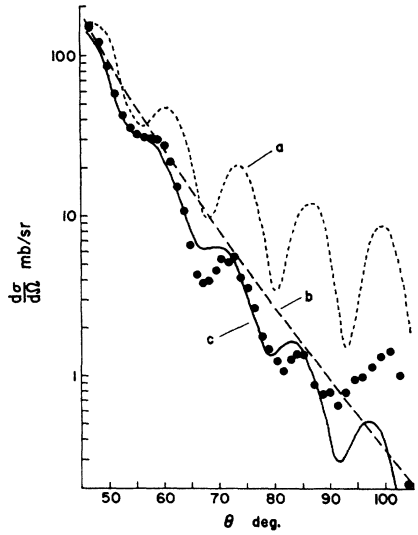

FIG. 9. ^{14}N-^{16}O data at 18.3 MeV (c.m. system). Curve (a) is the sharp-cutoff approximation for $r_0=1.65$ fm. Curve (b) is the rounded cutoff approximation with $r_0=1.65$ fm, $a=0.07$. Curve (c) is the three-parameter model with $r_0=1.65$ fm, $a=0.05$, $\Delta=0.9$.

and L_{cut} is defined by

$$L_{\mathrm{cut}}(L_{\mathrm{cut}}+1)=2mR^2\hbar^2[E-(Z^2e^2)/R]$$

and

$$R=r_0(A_1{}^{1/3}+A_2{}^{1/3}).$$

Finally, we choose $L_{\max}$ such that $\mathrm{Im}\alpha_{L_{\max}}$ is ≤ 0.001. Our free parameters are then r_0, a, and Δ and relate, respectively, to the nuclear radius, the surface thickness, and the magnitude of the real nuclear phase shift.

The differential cross section for identical spin 1 charged nuclear particles is

$$d\sigma/d\Omega=\tfrac{2}{3}|f_C(\theta)+f_C(\pi-\theta)+f_n(\theta)+f_n(\pi-\theta)|^2$$
$$+\tfrac{1}{3}|f_C(\theta)-f_C(\pi-\theta)+f_n(\theta)-f_n(\pi-\theta)|^2,$$

where $f_C(\theta)$ is the Coulomb amplitude. However, we have

$$f_n(\theta)=(-1)^L f_n(\pi-\theta),$$

since

$$P_L(\theta)=(-1)^L P_L(\pi-\theta).$$

So we get,

$$d\sigma/d\Omega=\tfrac{2}{3}|f_C(\theta)+f_C(\pi-\theta)+2f_n(\theta)_{\mathrm{even}}|^2$$
$$+\tfrac{1}{3}|f_C(\theta)-f_C(\pi-\theta)+2f_n(\theta)_{\mathrm{odd}}|^2,$$

where $f_n(\theta)_{\mathrm{even}}$ is summed over only the even L values and $f_n(\theta)_{\mathrm{odd}}$ over only the odd L values. For ^{14}N-^{16}O scattering the differential cross section expression is much simpler,

$$d\sigma/d\Omega=|f_C(\theta)+f_n(\theta)|^2.$$

A computer program with initially only r_0 and a as free parameters ($\Delta=0$) fitted the experimental data and calculated the average χ^2 per point. We then

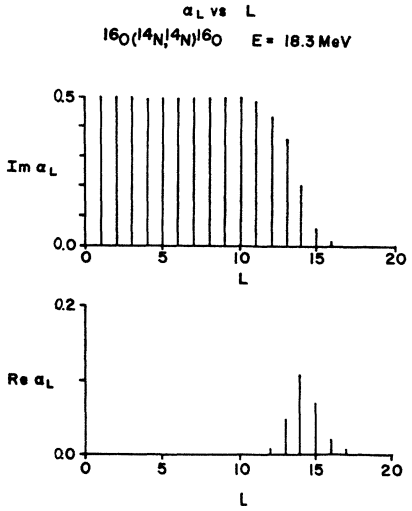

FIG. 10. Dependence of α_L with L for the diffraction-model fit to the data at 18.3 MeV. The value of L_{cut} for this energy is ~14.5.

incremented the parameters by ±0.01 (occasionally larger amounts) and repeated the calculations. In this manner we did obtain a fairly detailed grid of parameter values from which we selected the set with the lowest χ^2.

With the two-parameter diffraction model, we generally described the ^{14}N-^{14}N data adequately for energies less than ~14 MeV. At higher energies, the three-parameter model was necessary and resulted in fits to the data comparable to the four-parameter optical-model fits. See Table I and Fig. 7.

No single set of parameters (r_0, a, Δ) describes the ^{14}N-^{14}N experimental results satisfactorily over a wide energy range. However, when we use three parameters, the minima in χ^2 occur for nearly the same parameter values (see Table I).

At high energies for ^{14}N-^{14}N scattering, the diffraction model predicted 90° cross sections well below the measured values if parameters derived from the low-energy data were used at higher energies. By using a smaller radius parameter r, we partially compensate for this drop, but at the expense of poorer fits at other angles.

For ^{14}N-^{16}O scattering, we could not with two free parameters reproduce both the interference pattern of the angular distributions and the over-all trend of the cross section with angle. The sharp-cutoff approximation ($a=0.0$) gave angular distributions with correctly located maxima and minima, but the cross sections were far too high (see curve a of Fig. 9). For a nonzero value for a, the program obtains a better fit to the average cross section, but at a loss of the detailed structure (curve b of Fig. 9). The introduction of some nonzero real nuclear phase shift spread over a few L values near the surface (curve c of Fig. 9) resulted in much better detailed fitting of the angular distributions. Figure 10 shows the resulting values of Reα_L and Imα_L as a function of L for these data at 18.3 MeV. With this three-parameter model, we find a single set of parameters: $r_0=1.65$ fm, $a=0.05$, and $\Delta=0.9$, which represented the data fairly well over a wide range of energies. See Table II and Fig. 8.

This model suggests that in grazing collisions, the surface is partially absorbing and partially transmitting, or equivalently, the wave is partially attenuated (the imaginary component of nuclear phase) and partially shifted in the real component of nuclear phase.

CONCLUSIONS

The optical-model and the modified diffraction-model fits correspond to nuclei which are strongly absorbing in the interior and partially absorbing and partially refracting near the surface. At energies just above the Coulomb barrier this description appears adequate, but is unsatisfactory at the highest energies and at the most backward angles.

The two simple models are successful at low energies because little interpenetration arises, but fail at higher energies where the forces and distortions resulting from deep penetration are not so simply parameterized.

The more sophisticated models recently proposed[2–4] may result in improved fits to the data. A soft core at short range would have the most direct effect on low L waves, since they best sense the nuclear interior. The low L waves are also most sensitively felt in the angular distributions at angles near 90°.

The absorptive core determines the peak-to-valley ratio of the diffraction pattern. Since ^{14}N-^{16}O scattering has more open reaction channels than does ^{16}O-^{16}O, we should expect a wider and/or blacker core which would lead to a reduced peak-to-valley ratio for the interference peaks. This attenuation of the interference effects would again be more pronounced in the ^{14}N-^{14}N case than in the ^{14}N-^{16}O case, since ^{14}N-^{14}N has even more open channels than does ^{14}N-^{16}O. For a similar reason in our optical model the imaginary potential for ^{14}N-^{14}N is more than a factor of 3 deeper than the ^{14}N-^{16}O imaginary potential (see Tables I and II).

Finally, the ^{14}N-^{16}O data perhaps suggest some narrow structure, 100–200 keV wide, at higher energies (see Fig. 6). Here again is a feature which is prominent for ^{16}O-^{16}O at higher energies, is not so evident in the ^{14}N-^{16}O data, and is absent for ^{14}N-^{14}N. No satisfactory account of fine structure yet exists.

ACKNOWLEDGMENTS

I wish to express my thanks to Dr. H. T. Richards for his assistance and guidance on this work and to Dr. C. H. Blanchard for helpful discussions of the theoretical aspects. I also wish to thank all the members of Dr. Richards' research group for their assistance in data collection.